.

Time domain characteristics of wave motion in dispersive and anisotropic continuum acoustic metamaterials

Zhaojun Wang and Xiaoming Zhou

Citation: J. Acoust. Soc. Am. **140**, (2016); doi: 10.1121/1.4971330
View online: http://dx.doi.org/10.1121/1.4971330
View Table of Contents: http://asa.scitation.org/toc/jas/140/6
Published by the Acoustical Society of America

Time domain characteristics of wave motion in dispersive and anisotropic continuum acoustic metamaterials

Zhaojun Wang and Xiaoming Zhou[a)]
Key Laboratory of Dynamics and Control of Flight Vehicle, Ministry of Education and School of Aerospace Engineering, Beijing Institute of Technology, Beijing 100081, China

(Received 5 July 2016; revised 29 October 2016; accepted 20 November 2016; published online 15 December 2016)

The authors study the wave propagation in continuum acoustic metamaterials whose all or not all of the principal elements of the mass tensor or the scalar compressibility can be negative due to wave dispersion. Their time-domain wave characteristics are particularly investigated by the finite-difference time-domain (FDTD) method, in which algorithms for the Drude and Lorentz dispersion pertinent to acoustic metamaterials are provided necessarily. Wave propagation nature of anisotropic acoustic metamaterials with all admissible material parameters are analyzed in a general manner. It is found that anomalous negative refraction phenomena can appear in several dispersion regimes, and their unique time-domain signatures have been discovered by the FDTD modeling. It is further proposed that two different metamaterial layers with specially assigned dispersions could comprise a conjugate pair that permits wave propagation only at specific points in the wave vector space. The time-domain pulse simulation verifies that acoustic directive radiation capable of modulating radiation angle with the wave frequency can be realized with this conjugate pair. The study provides the detailed analysis of wave propagation in anisotropic and dispersive acoustic mediums, which makes a further step toward dispersion engineering and transient wave control through acoustic metamaterials.
[http://dx.doi.org/10.1121/1.4971330]

[MRH] Pages: 4276–4287

I. INTRODUCTION

Dispersion and anisotropy are inherent physical properties of acoustic metamaterials consisting of complex man-made microstructures. Dispersion arises from the local resonance of microstructures, through which acoustic metamaterials extrude the mass density or the compressibility into the negative-value space. Anisotropic wave property naturally exhibited by the structured metamaterials provides an additional degree of freedom for acoustic manipulation. Both features make acoustic metamaterial become an excellent approach to the wave-control realization, and great advances have been made in recent years.[1–3] Different structural types of acoustic metamaterials, including the bulk composite,[4,5] the discrete mass-spring structure,[6–8] the membrane structure,[9,10] the resonant cavity,[11,12] the coiling-channel structure,[13–15] and the chiral structure,[16] etc., have been proposed to achieve various wave-control functionalities, such as low-frequency acoustic isolation and absorption,[17] acoustic cloaking,[18–20] acoustic super-resolution imaging,[21,22] and non-reciprocal acoustic transmission,[23,24] etc.

The time-harmonic analyses upon metamaterial-based acoustic controlling mediums are frequently employed, which have shown their value in the proof-of-concept investigations, as concerned in most of the aforementioned studies. The time-domain characteristics of wave phenomenon in acoustic metamaterials are rarely paid attention to. However, there exist at least two circumstances where the transient analyses of metamaterials may be of great significance. One refers to the case in which the time-harmonic scenario is mismatched to practical environments. For example, in medical focused imaging and underwater sonar detection the short pulse excitations are commonly used. The other one lies in the case where the unique time-domain characteristics of metamaterials may provide surprising solutions to the bottlenecks of hindering the metamaterial applications. As an example, the material loss blocks the ultimate realization of super-resolution focusing by metamaterials. By smart use of the pulse excitation, lossy metamaterials may break the diffraction limit in the initial regime of the time domain.[25] The facts mentioned above state the objective demand of studies on the time-domain behaviors of acoustic metamaterials.

Acoustic metamaterials possess complex microstructures, which lead to complex dynamics on the micro scale. However, due to the fact that the overall property is dominated by the local behaviors of the cell structure,[26] metamaterials can be homogenized to be acoustic continua following the linear acoustic equation, whose material parameters involve a tensor mass density and a scalar compressibility. Under the homogenization assumption, the dispersion and anisotropy of structural metamaterials have been translated into the frequency-dependent material parameters and the tensorial feature of the inertial mass of their continua. Regarding dispersions, two classical Drude[27,28] and Lorentz[6,11] behaviors are commonly encountered, where negative inertial mass and negative compressibility can be well defined. Consequently, the continuum-material concept

[a)]Electronic mail: zhxming@bit.edu.cn

provides a phenomenological and convenient way to evaluate the time-domain characteristics of structural metamaterials by analyzing their continua assigned with either Drude or Lorentz dispersion models.

As a time-domain technique, finite-difference time-domain (FDTD) method naturally treats and calculates impulsive response of a dynamic system. The FDTD method has enjoyed a long history of success in computational electromagnetics (EMs),[29] and has been later extended to either non-dispersive or dispersive acoustic equations. In the non-dispersive realm, FDTD has been successfully developed for applications in acoustic imaging,[30] acoustic communication devices,[31] room acoustics,[32] phononic crystal,[33] etc. For acoustic materials whose damping is nontrivial, dispersive FDTD modeling is necessarily considered, for example, in realms of the ultrasonic imaging in biological tissues, which can be characterized by lossy acoustic materials following the Debye relaxation model[34] or frequency-dependent power law model,[35] etc. In contrast, acoustic Drude and Lorentz dispersions of the interest in this work have never been observed previously in natural materials. Therefore, there is no motivation to introduce them to the FDTD study until acoustic metamaterials emerged in the past decade. Now, rapid development of acoustic metamaterial design and their potential applications have made an urgent request for FDTD study of the Drude and Lorentz dispersive materials. To the best of our knowledge, those studies have not been comprehensively conducted yet.

As a preliminary study of the issue, in this work we develop a numerical tool based on the FDTD method to solve a general acoustic equation, where the partial or full diagonal elements of the mass density tensor or the scalar compressibility are dispersive, obeying either the Drude or Lorentz models. The details of algorithms are illustrated in Sec. II. In Sec. III, dispersion and anisotropy properties of continuum acoustic metamaterials are discussed in a general manner and their time-domain signatures are examined by the FDTD modeling. In Sec. IV, two different metamaterial layers with specially assigned dispersions are studied, which could comprise a conjugate pair that permits wave propagation in only two symmetry points in the wave vector space. The conclusion is made in Sec. V.

II. FDTD ALGORITHMS OF CONTINUUM ACOUSTIC METAMATERIALS

A. Basic equations of anisotropic acoustic medium

The time-harmonic ($e^{-i\omega t}$) acoustic equations for an anisotropic medium are written as

$$\nabla \cdot \mathbf{v} = -\kappa^{-1}(\omega)\frac{\partial p}{\partial t}, \tag{1}$$

$$\nabla p = -\boldsymbol{\rho}(\omega)\frac{\partial \mathbf{v}}{\partial t}, \tag{2}$$

where the mass density $\boldsymbol{\rho}(\omega)$ is a second-order tensor and the compressibility $\kappa(\omega)$ is a scalar. As a result of the material dispersion, they are the functions of the frequency ω. Without the loss of generality, we consider the two-dimensional (2D) scenario to examine the time-domain features of acoustic metamaterials. In the 2D case, assume that the $\boldsymbol{\rho}$ tensor is diagonalizable in the x-y space, namely, written as $\boldsymbol{\rho} = \mathrm{diag}[\rho_x, \rho_y]$. For a general representation, let the symbol Γ denote either ρ_x, ρ_y, or κ^{-1}. Introducing the constant Γ_∞ and polarization parameter $\chi(\omega)$ associated to Γ, we define

$$\Gamma(\omega) = \Gamma_\infty[1 + \chi(\omega)]. \tag{3}$$

In Eq. (3), the Drude and Lorentz dispersions will be considered for locally resonant metamaterials, from which negative material parameters can be well defined. For the Drude dispersion model, the polarization parameter $\chi(\omega)$ takes

$$\chi(\omega) = \frac{\omega_c^2}{\omega(j\gamma - \omega)}, \tag{4}$$

and for the Lorentz dispersion model $\chi(\omega)$ takes

$$\chi(\omega) = \frac{\eta\omega_0^2}{\omega_0^2 - \omega^2 + 2j\gamma\omega}, \tag{5}$$

where γ is the dissipation factor.

Referring back to acoustic Eqs. (1) and (2), we can write their time-domain forms as

$$\nabla \cdot \mathbf{v} = -\kappa^{-1}(t) * \frac{\partial p}{\partial t}, \tag{6}$$

$$\nabla p = -\boldsymbol{\rho}(t) * \frac{\partial \mathbf{v}}{\partial t}, \tag{7}$$

where the star operator on the right-hand side is referred to as the convolution operation. The corresponding time-domain polarization parameter $\chi(t)$ can be obtained by inverse Fourier transformation of Eqs. (4) and (5), yielding

$$\chi(t) = \frac{\omega_c^2}{\gamma}(1 - e^{-\gamma t})H(t) \tag{8}$$

for the Drude dispersion, and

$$\chi(t) = \alpha e^{-\gamma t}\sin(\beta t)H(t) \tag{9}$$

for the Lorentz dispersion, where $\beta = \sqrt{\omega_0^2 - \gamma^2}$, $\alpha = \eta\omega_0^2/\beta$, $H(t)$ is the Heaviside function. In Sec. II C, we provide the numerical approach of solving Eqs. (6) and (7) together with Eqs. (8) and (9) based on the FDTD method.

The simulation model of our interest is shown in Fig. 1, where the anisotropic and dispersive medium governed by Eqs. (6) and (7) is located inside a background medium that is dispersionless. The computational domain is truncated by the perfectly matched layers (PMLs) that serve as acoustic absorption materials. For the completeness of the work, the FDTD algorithms for the dispersionless medium will be briefly introduced. The finite-difference formulations of acoustic PML have also been provided and arranged in Appendix A.

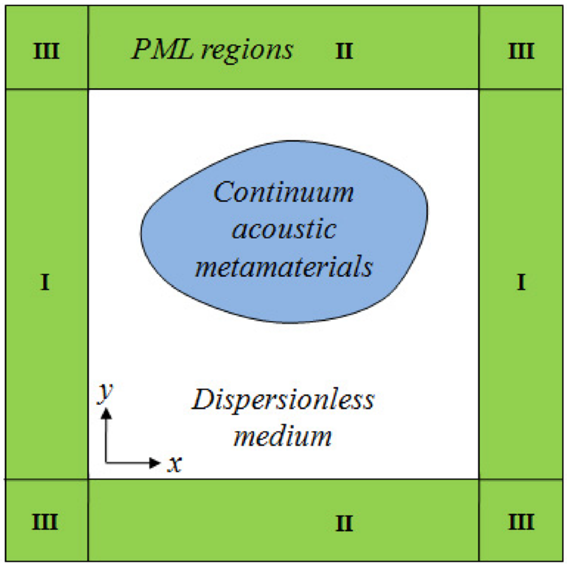

FIG. 1. (Color online) Schematics of the computational domain in which anisotropic and dispersive acoustic metamaterials located inside a dispersionless background medium that is surrounded by the PMLs.

B. FDTD algorithm of the dispersionless medium

The FDTD method employing the Yee algorithm[36] is a grid-based modeling technique and can be used for more than just Maxwell's equations. In an extension version to linear acoustics,[37] pressure p and particle velocities v_x, v_y are discretized using central-difference approximations to the space and time partial derivatives, as schematically shown in Fig. 2.

Using the same spatial discretization steps in the Cartesian staggered grids results in $\Delta x = \Delta y = \delta$. The time interval is denoted by Δt. δ and Δt need to satisfy the Courant stability condition[29]

$$\Delta t \le \frac{\delta}{\sqrt{2} c_0}, \tag{10}$$

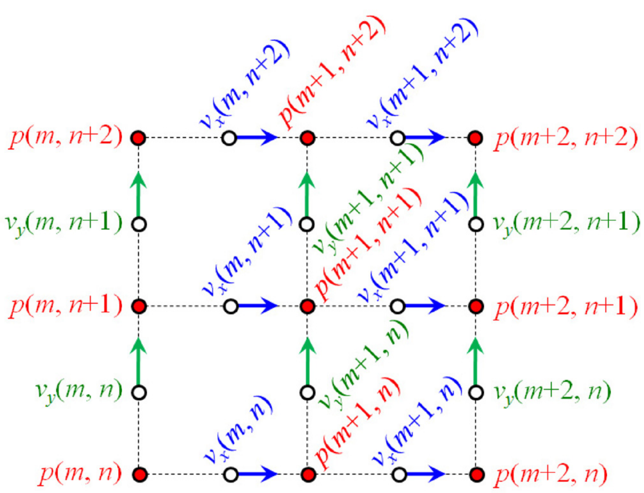

FIG. 2. (Color online) The Cartesian Yee grid used in the present acoustic FDTD study in which the pressure p and particle velocities v_x and v_y are discretized using central-difference approximations to the space and time partial derivatives.

where c_0 is the sound velocity. According to Fig. 2, acoustic pressure p is determined at the grid positions $(m\delta, n\delta)$ and the time $q\Delta t$, given by

$$p(x, y, t) = p^q[m, n] = p(m\delta, n\delta, q\Delta t), \tag{11}$$

where m, n, and q are integer numbers. The particle velocities, v_x and v_y, are determined as follows:

$$v_x(x, y, t) = v_x^q[m, n] = v_x(m\delta + \delta/2, n\delta, q\Delta t + \Delta t/2), \tag{12}$$

$$v_y(x, y, t) = v_y^q[m, n] = v_y(m\delta, n\delta + \delta/2, q\Delta t + \Delta t/2). \tag{13}$$

Based on the grid approximation defined above, the finite-difference formulations of acoustic Eqs. (1) and (2) in the dispersionless case are written as

$$v_x^{q+1}[m, n] = v_x^q[m, n] - \rho_x^{-1} \frac{\Delta t}{\delta} \left(p^q[m+1, n] - p^q[m, n]\right), \tag{14}$$

$$v_y^{q+1}[m, n] = v_y^q[m, n] - \rho_y^{-1} \frac{\Delta t}{\delta} \left(p^q[m, n+1] - p^q[m, n]\right), \tag{15}$$

$$\begin{aligned} p^{q+1}[m, n] = p^q[m, n] - \kappa \frac{\Delta t}{\delta} \big(& v_x^q[m+1, n] \\ & - v_x^q[m, n] + v_y^q[m, n+1] - v_y^q[m, n]\big). \end{aligned} \tag{16}$$

C. FDTD algorithm of dispersive and anisotropic continuum metamaterials

Going back to acoustic Eqs. (6) and (7) for dispersive mediums, we can write straightforwardly their finite-difference approximations in the Cartesian grid space

$$\begin{aligned} &\kappa^{-1} * p^{q+1}[m, n] - \kappa^{-1} * p^q[m, n] \\ &\quad = -\frac{\Delta t}{\delta} \big(v_x^q[m+1, n] - v_x^q[m, n] \\ &\qquad + v_y^q[m, n+1] - v_y^q[m, n]\big), \end{aligned} \tag{17}$$

$$\begin{aligned} &\rho_x * v_x^{q+1}[m, n] - \rho_x * v_x^q[m, n] \\ &\quad = -\frac{\Delta t}{\delta} \left(p^q[m+1, n] - p^q[m, n]\right), \end{aligned} \tag{18}$$

$$\begin{aligned} &\rho_y * v_y^{q+1}[m, n] - \rho_y * v_y^q[m, n] \\ &\quad = -\frac{\Delta t}{\delta} \left(p^q[m, n+1] - p^q[m, n]\right). \end{aligned} \tag{19}$$

In the following, we take Eq. (17) as an example to present the finite-difference approach to the convolution operator. The method can be equally used for Eqs. (18) and (19).

When the compressibility is dispersive, $\kappa^{-1}(\omega) = \kappa_\infty^{-1}[1 + \chi(\omega)]$, the convolution operation $\kappa^{-1}(t) * p(t)$ encountered in Eq. (17) is defined as

$$\kappa^{-1}(t) * p(t) = \kappa_\infty^{-1} p(t) + \kappa_\infty^{-1} \int_0^t p(t - \tau)\chi(\tau) \mathrm{d}\tau, \tag{20}$$

where the causality requires $p(t)=0$ when $t<0$. To implement the integration appearing in Eq. (20), the recursive-convolution (RC) formulation[38,39] can be adopted to approximate continuous time function $p(t)$ by a constant value over each time-step Δt. It is worth noting that the RC formulation of interest is numerically stable and sufficiently accurate in the case of fine meshes as ensured in the examples of this work. The details of the RC algorithms have been provided in Appendix B.

The RC techniques presented in Appendix B can be applied in the same procedure to the remaining Eqs. (18) and (19). Consequently, the time-domain responses of dispersive and anisotropic acoustic metamaterials can be modeled based on the presented algorithms. In Sec. III, the FDTD method is used to analyze the wave reflection and transmission for a pulse obliquely incident from the air onto a Drude dispersive metamaterial. Different dispersive parameters for ρ_x, ρ_y, and κ^{-1} will be particularly investigated.

III. TIME-DOMAIN MODELING OF DISPERSIVE AND ANISOTROPIC CONTINUUM ACOUSTIC METAMATERIALS

The one-interface problem will be examined in this section, where the geometric space is divided into two half-spaces occupied, respectively, by the dispersive metamaterial and a nondispersive air medium. In Sec. III A, the propagation or non-propagation nature of waves in acoustic metamaterials with all admissible material parameters will be discussed in a general manner. The study in Sec. III B is devoted to numerical experiments based on the FDTD modeling in order to disclose the time-domain characteristics of continuum acoustic metamaterials. Comparison analyses of FDTD modeling results and theoretical predictions based on dispersion curves will be also provided.

A. Material space of anisotropic acoustic metamaterials

Suppose that the half-space with the positive x coordinate is occupied by the metamaterial. In the time-harmonic case, the pressure field of a plane wave is of the following form:

$$p=p_0 e^{i(k_x x+k_y y-\omega t)}, \tag{21}$$

where k_x and k_y are, respectively, the x and y components of the wave vector, and ω is the oscillation frequency. Substituting Eq. (21) into acoustic Eqs. (1) and (2), one can obtain the dispersion equation for an anisotropic medium

$$k_x^2+\frac{\rho_x}{\rho_y}k_y^2=\frac{\rho_x}{\kappa}\omega^2. \tag{22}$$

In the lossless case, the sign of the solution k_x^2 to Eq. (22) can be used to distinguish the wave-propagating nature. It means that $k_x^2>0$ corresponds to the propagating solutions, while $k_x^2<0$ means the evanescent (non-propagating) solutions. The positive k_x^2 solutions to Eq. (22) have been illustrated with color regions in a three-dimensional (3D) material space using ρ_x, ρ_y, and κ as Cartesian coordinates, as shown in Fig. 3. Empty regions denote the non-propagating case. For all-positive material parameters, like those in most natural materials, there exists a cutoff value $k_c=\omega\sqrt{\rho_y/\kappa}$, which is the solution to the case $k_x(k_y=k_c)=0$ and separates the propagating wave and evanescent wave spectra. To show this cutoff effect in the material space (Fig. 3), the radial direction is defined as a new coordinate k_y; then the cutoff behavior lets an internal region ($k_y<k_c$) to be propagating (the color gray). The same cutoff effect happens in the all-negative case (the color red), where ρ_x, ρ_y, $\kappa<0$. In quadrants with $\rho_x>0$, $\rho_y<0$, $\kappa<0$, or $\rho_x<0$, $\rho_y>0$, $\kappa>0$ (the color violet), the cutoff effect is reversed, so that this anti-cutoff effect leads to the presence of propagation behavior in an external region ($k_y>k_c$). In another case of $\kappa\rho_y>0$ and $\rho_x\rho_y<0$ (the color green), waves are always propagating for any k_y; while for $\kappa\rho_y<0$ and $\rho_x\rho_y>0$, waves are always prohibited. The above mentioned anomalous behaviors enabled by acoustic metamaterials are as rich as observed in EM indefinite media,[40] and would provide a flexible degree of freedom for acoustic manipulation. Further analyses will be given on the basis of the FDTD simulations.

B. FDTD modeling of dispersive and anisotropic acoustic metamaterials

The FDTD simulation model is shown in Fig. 4(a), where the dispersive metamaterial occupies the positive x region, and the adjacent half space is the air with the mass density $\rho_0=1.25\,\text{kg/m}^3$ and sound velocity $c_0=343\,\text{m/s}$. Simulation regions are bordered with the PMLs, which are not shown for concise illustration. Acoustic excitation is emitted from the line source of length $l=12\,\text{cm}$, whose geometric location has been indicated in the figure. The pulse signal of the source is given in terms of the pressure by

$$p_s(\mathbf{x},t)=\exp\left[-\frac{|\mathbf{x}-\mathbf{x}_c|^2}{l_\tau^2}\right]\left[1-\cos\left(\frac{2\pi f_{\mathrm{ctr}}t}{N}\right)\right]\sin(2\pi f_{\mathrm{ctr}}t), \tag{23}$$

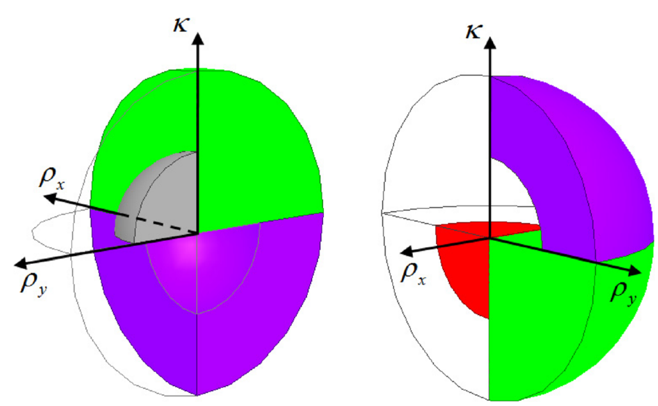

FIG. 3. (Color online) Propagating (color) or non-propagating (empty) nature of anisotropic acoustic metamaterials designated in a 3D material space using their mass densities ρ_x, ρ_y, and compressibility κ as Cartesian coordinates.

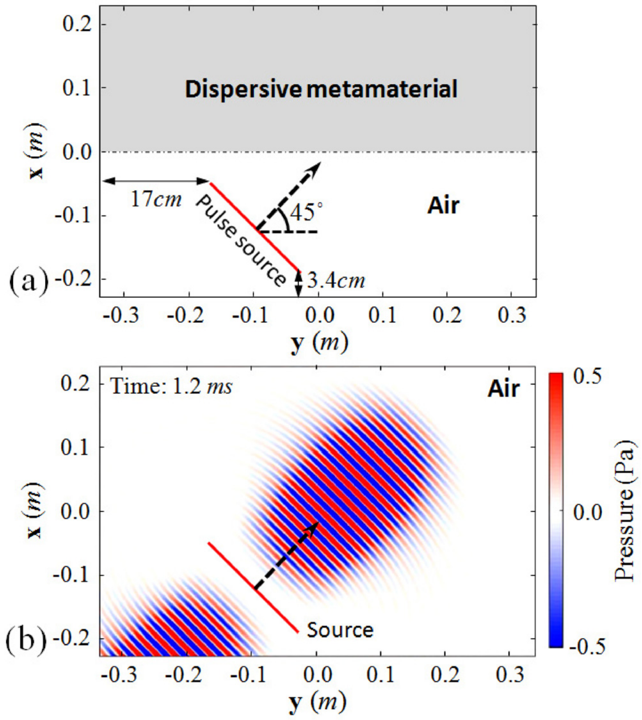

FIG. 4. (Color online) (a) Schematics of the FDTD simulation model for pulse wave refraction by anisotropic and dispersive acoustic metamaterials. Acoustic tone burst is emitted in the air by a line source having the Gaussian pressure distribution. (b) Simulated pressure distribution of incident pulse wave in the air captured at the instant time 1.2 ms, where the cycle number $N = 20$ and the central frequency $f_{ctr} = 17$ kHz are used for the tone burst signal.

where the first term on the right-hand side describes the Gaussian distribution of the pressure in the source line, $\mathbf{x}_c$ is the coordinate of the central point in the line, and l_τ/l is taken as 0.42. The remaining terms refer to the time variation that describes the tone burst signal, where f_{ctr} is the central frequency and the cycle number $N = 20$ is used. Figure 4(b) shows the pressure field of acoustic source in the air captured at an instant time 1.2 ms, where the central frequency f_{ctr} is taken as 17 kHz. Acoustic source defined by the form (23) is clearly seen to produce a spatially confined pulse beam, which is suitably used in the following study.

Constant negative material parameters violate the causality, thus are not permitted in the time-domain modeling. Without the loss of generality, acoustic metamaterials considered in the FDTD simulator take the Drude dispersion model with the following parameters:

$$\rho_x = 6\rho_0\left(1 - \frac{f_c^2}{f(f - i\gamma)}\right), \quad \rho_y = \rho_0\left(1 - \frac{4f_c^2}{f(f - i\gamma)}\right),$$
$$\frac{1}{\kappa} = \frac{1}{3\kappa_0}\left(1 - \frac{2.25f_c^2}{f(f - i\gamma)}\right), \tag{24}$$

where $f_c = 10$ kHz and $\gamma/f_c = 10^{-4}$. Different dispersive parameters for ρ_x, ρ_y, and κ^{-1} are chosen to pursue the diverse propagation behaviors: all-negative, partially negative with anti-cutoff and never cutoff, and all-positive ones at different frequency regions in this single metamaterial. When these frequency-dependent material parameters [Eq. (24)] are considered, the eigenfrequency solutions f to dispersion Eq. (22) for various k_x and k_y normalized to $k_a = 2\pi f_c/c_0$ can be computed as shown by the contour plot in Figs. 5(a)–5(d) corresponding, respectively, to frequency regions $f/f_c \in (0.5, 1.0)$, $f/f_c \in (1.0, 1.5)$, $f/f_c \in (1.5, 2.0)$, and $f/f_c \in (2.0, 7.0)$.

In the region of the frequency below f_c where all parameters ρ_x, ρ_y, and κ are negative, it can be observed from Fig. 5(a) that the frequency is a concave function of k_x and k_y satisfying $\nabla^2 f(k_x, k_y) < 0$ and reaches the maximum at the central point of the k space. We note that this concave profile, contrary to the convexity in conventional all-positive mediums, is the origin of opposite directions of group and phase velocities. For further explanation, the isofrequency line is examined at a specific case $f(k_x, k_y) = 0.9f_c$ for both the metamaterial (the solid line) and the air (the dashed circle line). In the excitation case of $k_{0x} = k_{0y}$ as concerned in Fig. 4(a), the group velocity v_g, which is defined as the gradient of the frequency over the k space $v_g = \nabla f(k_x, k_y)$, would point inwards because of the concave nature of the frequency contour, and the phase velocity v_p is directed outwards. As a result, wave energy propagates forward but with a negative-refraction angle, while the phase advances backward due to $k_x < 0$, as marked in Fig. 5(a). The rules governing the above physical process can be generalized as follows. For an incident wave having the phase velocity v_0, the wave vector component k_x in the metamaterial is determined from the physical law that the transverse components of wave vector should be conserved, i.e., $k_y = k_{0y}$. The group velocity v_g, which is normal to the isofrequency line, is oriented toward the direction of frequency increasing; Meanwhile, the forward component (the y component in this study) of v_g must be positive due to causality.

We perform numerical experiments based on the FDTD to verify the refraction phenomenon predicted above and disclose the time-domain signatures of anomalous wave refraction by metamaterials. The simulation environment shown in Fig. 4(a) is considered, where the incident pulse beam is set with $N = 20$ and $f_{ctr} = 0.9f_c$. Figure 5(e) shows the snapshot of acoustic pressure captured at the instant time 3.0 ms. It can be found that the phase velocity direction that is vertical to the wavefront indeed coincides with the predicted one. More information about the backward feature of the phase velocity and negative refraction of the wave group need be identified from the animation plot provided in the supplementary material.[41] The directions of phase advance v_p and group propagation v_g determined by FDTD modeling have been marked in Fig. 5(e), which coincide exactly with the prediction. In addition, special attention should be given to the variation of the envelope of nontrivial beam fields after the refraction. In the incident medium, the major axis of the ellipse-like beam envelope is in parallel to the group propagation direction. It may be presumed that the elliptic envelope is also bended in the same way as negative refraction of the wave group. However, the fact is that they are misaligned, although the beam profile is indeed bended negatively. Conclusively, the orientations of the beam envelope,

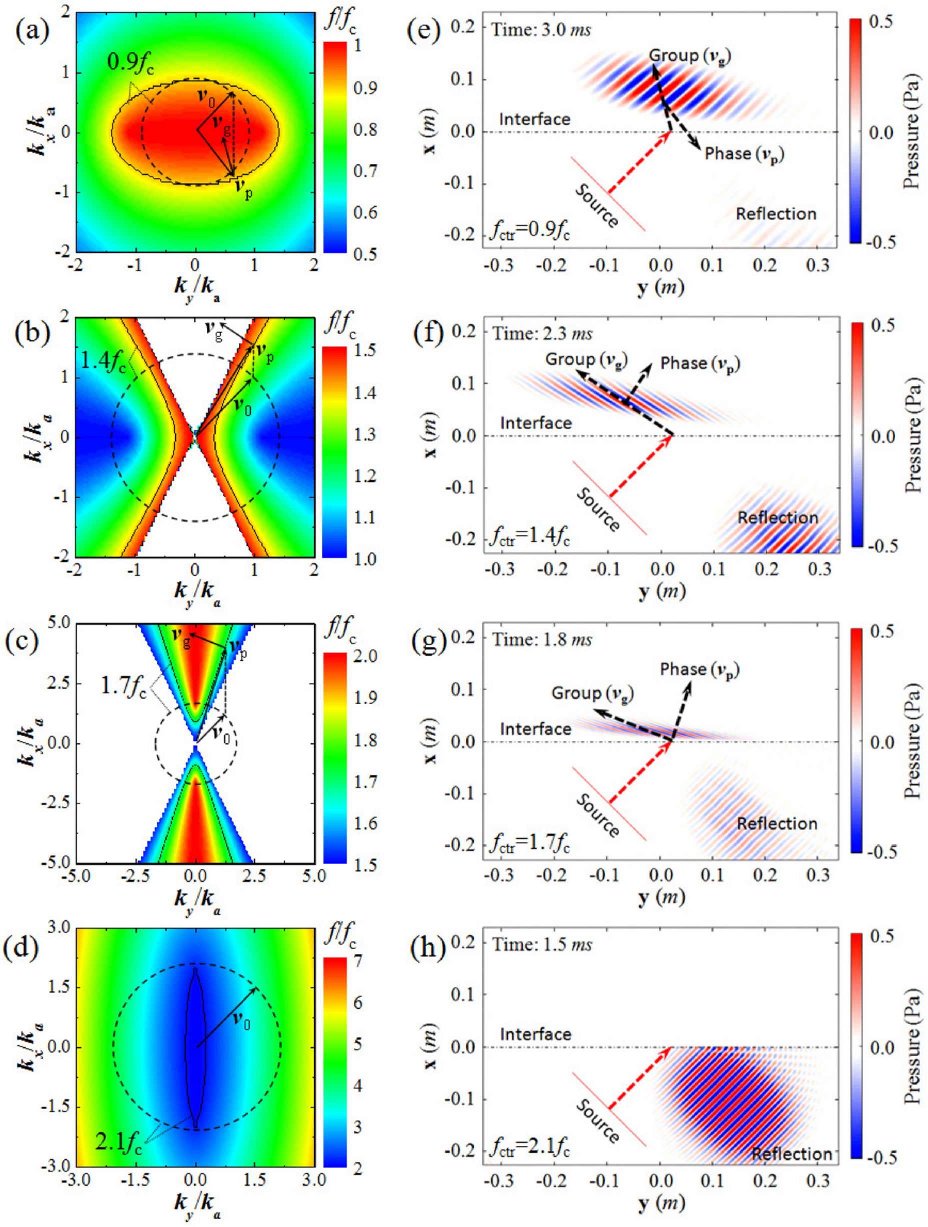

FIG. 5. (Color online) The diverse wave refraction phenomena observed in all-negative [(a) and (e)], partially negative with anti-cutoff [(b) and (f)] and never cutoff [(c) and (g)], and all-positive [(d) and (h)] frequency regions in a single anisotropic metamaterial as defined by Eq. (24). Left panels: contour plot of eigenfrequency solutions to dispersion Eq. (22) of the studied metamaterial, which are shown in four adjacent frequency regions: (a) $f/f_c \in (0.5, 1.0)$; (b) $f/f_c \in (1.0, 1.5)$; (c) $f/f_c \in (1.5, 2.0)$; (d) $f/f_c \in (2.0, 7.0)$. Right panels: The snapshot of acoustic pressure field in the case of different central frequencies (e) 0.9f_c, (f) 1.4f_c, (g) 1.7f_c, and (h) 2.1f_c of the incident pulse shows the typical wave refraction behaviors in different frequency regions.

phase, and group propagation directions of a refracted beam can be mutually different in a dispersive metamaterial.

Falling between f_c and 1.5f_c is the anti-cutoff region, in which $\rho_x > 0$, $\rho_y < 0$, $\kappa < 0$. Figure 5(b) shows the contour plot of frequency solutions to dispersion Eq. (22). For clear illustration of dispersion behavior, the isofrequency curve is concerned at a specific case 1.4f_c. It turns out to be hyperbola with the two vertices located at the k_y axis. Obviously, the hyperbolic curve of this kind supports the propagating mode in the wavenumber region beyond the cutoff $k_y = k_c$, which is the distance from the center to the vortex in Fig. 5(b). Figure 5(f) shows the snapshot of FDTD simulation results at time 2.3 ms when the pulse beam with $f_{ctr} = 1.4f_c$ is launched. It is found out[41] that, as in agreement to the prediction from the dispersion curve, the energy group of an acoustic beam is again refracted negatively. But the fact different from the all-negative case is in that the energy flux direction is almost vertical to the phase one, and the latter becomes forward in this case. In the next region between 1.5f_c and 2f_c, the parameters belong to the always propagating case. The isofrequency curve chosen at an arbitrarily frequency 1.7f_c is still hyperbolic [Fig. 5(c)], however the two vertices locate at the k_x axis in contrast to Fig. 5(b). This explains the never-cutoff effect, since k_x would always attain a real value for any k_y. The FDTD results in Fig. 5(g) shows that negative refraction of acoustic beam happens again, and their time-domain signatures are similar to the phenomenon in the anti-cutoff case [Fig. 5(f)].

In the region of the frequency beyond 2f_c, all parameters ρ_x, ρ_y, and κ are positive, which is the usual case in natural materials. The isofrequency curve chosen at 2.1f_c reveals the elliptic profile as shown in Fig. 5(d). Due to the strong anisotropy $\rho_x/\rho_y \approx 51.5$ in this example, the y component k_{0y} of the incident wave falls in the evanescent regime ($k_x^2 < 0$) of the metamaterial, resulting in the prohibited wave propagation. This has been demonstrated by the FDTD results shown in Fig. 5(h), where the incident pulse beam with the central frequency $f_{ctr} = 2.1f_c$ is totally reflected by the metamaterial.

In this part of the study, we explain physical properties of continuum metamaterials with all-negative, partially-negative, and all-positive material parameters in terms of numerical examples. Negative refractions are observed in three dispersion cases and their distinct time-domain characteristics have been clearly discovered. In Sec. IV, studies are devoted to an interesting transmission phenomenon found in a two-layer structure, of which one layer is the cutoff medium and the other is the anti-cutoff one having the same cutoff wavenumber.

IV. WAVE PROPAGATION IN THE k_C-CONJUGATE PAIR

Consider two anisotropic acoustic mediums (labeled with subscripts "1" and "2") whose material parameters satisfy

$$\rho_{1x}\rho_{2x} < 0, \quad \rho_{1y} = \rho_{2y} > 0, \quad \kappa_1 = \kappa_2 > 0. \tag{25}$$

We call them the k_c-conjugate metamaterial pair based on the fact that they share the same cutoff value of $k_c = \omega\sqrt{\rho_{1y}/\kappa_1} = \omega\sqrt{\rho_{2y}/\kappa_2}$, however exhibit the opposite, namely, cutoff and anti-cutoff, behaviors. In the k space, it means that the propagating regions of two mediums never overlap, but contact at only two symmetry points $k_x = 0$, $k_y = +k_c$ and $k_x = 0$, $k_y = -k_c$. Wave characteristics of the k_c-conjugate pair will be studied in this section.

A. Dispersion and wave transmission analyses

Consider the following parameters for a pair of materials:

$$\rho_{1x} = \rho_0, \quad \rho_{2x} = \rho_0\left(1 - \frac{2.25 f_c^2}{f(f - i\gamma)}\right);$$
$$\rho_{1y} = \rho_{2y} = 2\rho_0\left(1 - \frac{f_c^2}{f(f - i\gamma)}\right); \quad \kappa_1 = \kappa_2 = \kappa_0, \tag{26}$$

where we set $f_c = 10\,\text{kHz}$ and $\gamma/f_c = 10^{-4}$. When $f/f_c = 1.14$ is taken, the footprints of this k_c-conjugate pair in the k space are schematically shown in Fig. 6(a), where the isofrequency curves of the 1 and 2 mediums of the pair refer, respectively, to the borders of the ellipse (the color gray) and hyperbola (the color violet). It is obvious that their propagation-dominated areas never overlap, but contact at the points $k_x = 0$, $k_y = \pm k_c$. For clear explanation, consider only the positive regions of k_y hereafter.

It is readily found that the cutoff value k_c depends on the frequency

$$k_c = \frac{k_0}{f/f_c}\sqrt{2\left[(f/f_c)^2 - 1\right]}. \tag{27}$$

Equation (27) underlines that k_c can take any values between zero and $k_0 = \omega\sqrt{\rho_0/\kappa_0}$ when the frequency sweeps from f_c and $1.5f_c$. Thus, the k_c-conjugate pair can potentially be used as an acoustic filter, which suppresses all signals in the wavenumber domain $0 \le k_y \le k_0$, except with a certain

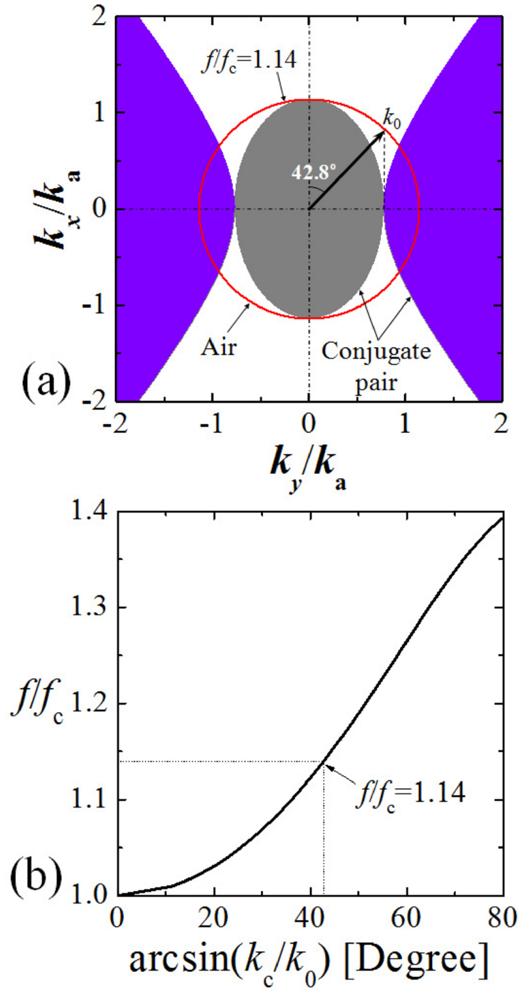

FIG. 6. (Color online) (a) Typical dispersion characteristics of the k_c-conjugate pair, one of which follows the cutoff (the color gray) dispersion, and the other belongs to the anti-cutoff (the color violet) one; they never overlap but contact at the cutoff points $k_x = 0$, $k_y = \pm k_c$. (b) The incident angle of waves that are permitted for propagation across the k_c-conjugate pair is determined by k_c and monotonically proportional to the wave frequency due to the inherent dispersion of metamaterials.

wavenumber component $k_y = k_c$. In other words, if a plane wave is incident at an angle θ on the pair, only the wave of the incident angle satisfying $\theta = \arcsin(k_c/k_0)$ is permitted for propagation. This specific angle θ is $42.8°$ in the case of $f/f_c = 1.14$ and varies monotonically with the operating frequency due to the metamaterial dispersion, as shown in Fig. 6(b).

The cutoff wavenumber $k_y = k_c$ is the only permitted point for propagation, while it is still necessary to analyze acoustic transmission amplitude across the pair at this point. The transmission coefficient T of two layers of anisotropic-mass acoustic mediums with thicknesses h_1 and h_2 is given by

$$T = \frac{2i\rho_0\rho_{1x}\rho_{2x}k_{0x}k_{1x}k_{2x}}{\rho_{1x}k_{1x}\cos(k_{1x}h_1)T_1 + \sin(k_{1x}h_1)T_2}, \tag{28}$$

where

$$T_1 = 2i\rho_0\rho_{2x}k_{0x}k_{2x}\cos(k_{2x}h_2) + (\rho_0^2k_{2x}^2 + \rho_{2x}^2k_{0x}^2)\sin(k_{2x}h_2), \tag{29}$$

$$T_2 = \rho_{2x} k_{2x} (\rho_0^2 k_{1x}^2 + \rho_{1x}^2 k_{0x}^2) \cos(k_{2x} h_2) - i\rho_0 k_{0x} (\rho_{1x}^2 k_{2x}^2 + \rho_{2x}^2 k_{1x}^2) \sin(k_{2x} h_2). \tag{30}$$

At the point $k_y = k_c$, the x components of wave vectors in the air and the pair are

$$k_{0x} = \sqrt{k_0^2 - k_c^2},\ k_{1x} = k_{2x} = 0. \tag{31}$$

We attempt to simplify Eq. (28) under the conditions of Eq. (31). To do this, assume k_{1x} and k_{2x} to be an infinitesimal value δ, instead of being zero as shown in Eq. (31). Then the following approximations can be obtained $\cos(k_{1x}h_1) \approx \cos(k_{2x}h_2) \approx 1$, $\sin(k_{1x}h_1) \approx \delta h_1$, and $\sin(k_{2x}h_2) \approx \delta h_2$. By use of these relations, Eq. (28) can be simplified as

$$T \approx \frac{2i\rho_0}{2i\rho_0 + (\rho_{1x}h_1 + \rho_{2x}h_2)k_{0x} + o(\delta)}. \tag{32}$$

To achieve high transmission at the limiting case $\delta \to 0$, the minimization of the term $(\rho_{1x}h_1 + \rho_{2x}h_2)k_{0x}$ in the denominator of Eq. (32) needs to be pursued. This usually requires that the thickness of the pair is as small as possible compared to the wavelength in the background medium. However, this is not a strict requirement, as concluded in the following example.

Choose a not sufficiently small thickness $h_1 = h_2 = 1$ cm for the pair used in Fig. 6. At this case, the total thickness of the pair is up to 0.58 times of the air wavelength at frequency f_c. Figure 7(a) shows the contour plot of transmission amplitude $|T|$ of the pair at different incident angle and frequency. Nearly total transmission in the vicinity of the θ - f curve (the dashed line) as provided previously in Fig. 6(b) is found, which demonstrates the minor influence of the term $(\rho_{1x}h_1 + \rho_{2x}h_2)k_{0x}$ even though the pair is thick. The underlying physics is similar to that observed in the near-zero-density metamaterials,[42] which also have the zero x component of the wave vector. The results can be seen more clearly in Fig. 7(b), which shows the line plot of transmission amplitude versus the incident angle for five different frequencies $f/f_c = 1.08$, 1.11, 1.14, 1.17, and 1.2. The maximum transmission in each curve corresponds to the point $k_y = k_c$, which is almost unity and slightly lowered as the frequency increases because of the enhanced thickness-to-wavelength ratio. The transmission on the left (right) side of the hilltop is lowered because they fall into the evanescent zone of the hyperbolic (elliptic) dispersion materials in the pair.

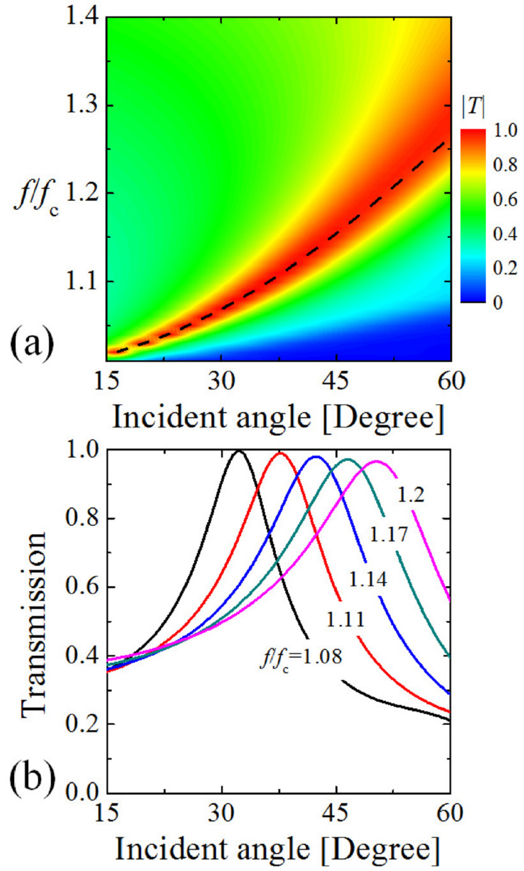

FIG. 7. (Color online) (a) Contour plot of transmission amplitude $|T|$ across the k_c-conjugate pair for plane acoustic waves with different incident angle and frequency; (b) line plot of transmission amplitudes against the incident angle in case of five different frequencies $f/f_c = 1.08$, 1.11, 1.14, 1.17, and 1.2.

B. FDTD modeling of acoustic radiation by the k_c-conjugate pair

The wave leakage by the pair at the single point $k_y = k_c$ and their monotonic dependency on the frequency can be verified by acoustic radiation simulation based on the FDTD. Take the wavelength λ_c in the air at frequency f_c as a measure. A point source is placed at a distance $\lambda_c/10$ to one side of the pair, and launches the tone burst signal in the following form:

$$p_s(t) = \left[1 - \cos\left(\frac{2\pi f_{ctr} t}{N}\right)\right] \sin(2\pi f_{ctr} t) \quad \text{with } N = 20. \tag{33}$$

On the other side of the pair, take the point that lies in the same surface normal with the source point as the origin. At the radius $10\lambda_c$ far from this origin, the time-domain signals of the pressure are computed based on the FDTD method and collected as a function of the radiation angle. They are then Fourier transformed to obtain the pressure fields in the frequency domain.

Figure 8 shows acoustic radiation patterns in the angular and frequency domains at different source central frequencies, $f_{ctr}/f_c = 1.08$, 1.11, 1.14, 1.17, 1.20, and 1.23. The θ - f curve in Fig. 6(b) is cited again by the dashed line as the reference. Since the acoustic field of a point source can be expressed as the field superposition of an infinite number of plane waves with different k_y, nearly complete transmission at only $k_y = k_c$ makes the pair behave like a leaky wave acoustic antenna, which operates in the manner that the radiation angle $\theta = \arcsin(k_c/k_0)$ can be varied with the source frequency. Results have been verified in Fig. 8, where the tight radiation spots are found at all examined cases and quite close to the predicted θ - f curve. In our previous study,[43] acoustic directive radiation modulated by frequency

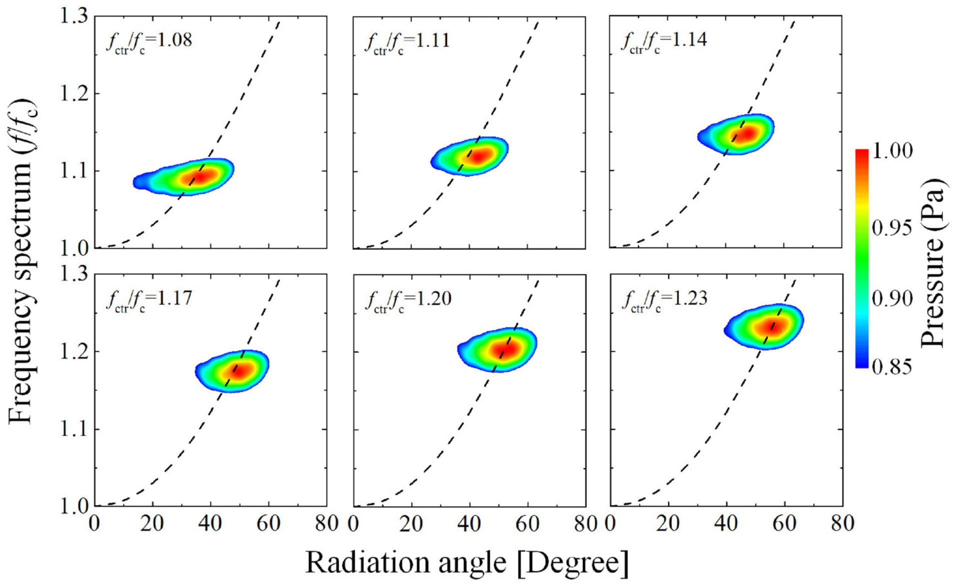

FIG. 8. (Color online) FDTD modeling results of acoustic radiation by the k_c-conjugate pair backed by a point pulse source operating at different central frequencies $f_{ctr}/f_c = 1.08$, 1.11, 1.14, 1.17, 1.20, and 1.23. Radiation patterns refer to the far-field pressure distributions in the angular and frequency domains and are in accordance to the θ - f curve predicted by Fig. 6(b).

has been realized by the spatial dispersion of dynamic mass density in thin-plate acoustic metamaterials. It is worth emphasizing here that the similar functionality has been realized by a k_c-conjugate pair without employing the spatial dispersion effect. This clearly reveals the powerfulness of dispersion engineering by anisotropic acoustic metamaterials.

V. CONCLUSIONS

In this work, we develop a FDTD-based simulation tool to study time-domain characteristics of anisotropic continuum acoustic metamaterials following either Drude or Lorentz dispersions. Wave propagation characteristics in acoustic metamaterials with all admissible material parameters are clearly addressed. Negative refraction phenomena have been found in three different dispersion regimes, and verified by the time-domain simulation using acoustic pulse beam as the excitation. It is found that the envelope orientation of the beam, and its phase and group velocity direction in the refracted medium, can be mutually different. We have also studied acoustic characteristics of the k_c-conjugate pair that permits wave propagation at only the cutoff wavenumber. Due to the inherent dispersion of the pair, the cutoff point varies monotonically with the frequency. These features let the k_c-conjugate pair to be an acoustic radiation device capable of modulating the radiation angle by the source frequency, as demonstrated by the FDTD simulation.

The developed numerical simulator based on the FDTD can be easily extended to the three-dimension case and could serve as a powerful tool to study the transient behavior of dispersive metamaterials. In the continued work, the metamaterial application under transient wave environment of practical engineering will be deeply explored with the help of this dispersive FDTD simulator.

ACKNOWLEDGMENTS

This work was supported by the National Natural Science Foundation of China (Grant Nos. 11521062, 11572039, and 11622215), and 111 project (Project No. B16003).

APPENDIX A: FDTD ALGORITHM OF THE PMLs

The PMLs serve as a non-reflection boundary designed to prevent the interference between the unwanted reflection waves and physical fields of the interest. The PML techniques are invented first for EM free-space simulation[44] and later adopted in acoustics. In a general case, the lossy acoustic equations including a dissipation factor α^d are expressed as

$$\nabla \cdot \mathbf{v} = -\kappa^{-1}\frac{\partial p}{\partial t} - \alpha^d p, \tag{A1}$$

$$\nabla p = -\rho\frac{\partial \mathbf{v}}{\partial t} - \alpha^d \rho\kappa\mathbf{v}. \tag{A2}$$

In order for the thorough impedance matching, the pressure can be decomposed to be p_x and p_y according to the rule $p = p_x + p_y$. Then Eqs. (A1) and (A2) can be modified as

$$-\kappa^{-1}\frac{\partial p_x}{\partial t} - \alpha_x p_x = \frac{\partial v_x}{\partial x}, \tag{A3}$$

$$-\kappa^{-1}\frac{\partial p_y}{\partial t} - \alpha_y p_y = \frac{\partial v_y}{\partial y}, \tag{A4}$$

$$-\rho\frac{\partial v_x}{\partial t} - \alpha_x \rho\kappa v_x = \frac{\partial p}{\partial x}, \tag{A5}$$

$$-\rho\frac{\partial v_y}{\partial t} - \alpha_y \rho\kappa v_y = \frac{\partial p}{\partial y}, \tag{A6}$$

where α_x and α_y are decomposed dissipation factors. Their values are different in PML regions I, II, and III of Fig. 1 and can be taken as[45]

$$\begin{cases} \alpha_x[m,n] = \left(\dfrac{M-1/2-m}{M-1/2}\right)^2 \alpha_x^{\max}, m = 0,1,\ldots,M-1 \\ \alpha_y[m,n] = 0 \end{cases} \quad \text{for region I,} \tag{A7}$$

$$\begin{cases} \alpha_x[m,n] = 0 \\ \alpha_y[m,n] = \left(\dfrac{N-1/2-n}{N-1/2}\right)^2 \alpha_y^{\max}, n = 0,1,\ldots,N-1 \end{cases} \quad \text{for region II,} \tag{A8}$$

$$\begin{cases} \alpha_x[m,n] = \left(\dfrac{M-1/2-m}{M-1/2}\right)^2 \alpha_x^{\max}, m = 0,1,\ldots,M-1 \\ \alpha_y[m,n] = \left(\dfrac{N-1/2-n}{N-1/2}\right)^2 \alpha_y^{\max}, n = 0,1,\ldots,N-1 \end{cases} \quad \text{for region III.} \tag{A9}$$

It is worth noting that M and N are total numbers of the PML grids. m and n are counted as starting from the outer boundary of the PML. For the sake of rapid wave dissipation within the PML, the exponential-difference approximation to the time partial derivatives should be used.[46] Take Eq. (A3) as an example; the finite-difference formulation of the left-hand side of Eq. (A3) is given by

$$\kappa^{-1}\frac{\partial p_x}{\partial t} + \alpha_x p_x = \frac{\alpha_x\left(p_x^{q+1} - p_x^q e^{-\alpha_x\kappa\Delta t}\right)}{1 - e^{-\alpha_x\kappa\Delta t}}. \tag{A10}$$

Applying the above exponential-difference approximation to Eqs. (A3)–(A6) yields

$$p_x^{q+1}[m,n] = e^{-\alpha_x[m,n]\kappa\Delta t} p_x^q[m,n] - \frac{1 - e^{-\alpha_x[m,n]\kappa\Delta t}}{\delta\alpha_x[m,n]}\left(v_x^q[m+1,n] - v_x^q[m,n]\right), \tag{A11}$$

$$p_y^{q+1}[m,n] = e^{-\alpha_y[m,n]\kappa\Delta t} p_y^q[m,n] - \frac{1 - e^{-\alpha_y[m,n]\kappa\Delta t}}{\delta\alpha_y[m,n]}\left(v_y^q[m,n+1] - v_y^q[m,n]\right), \tag{A12}$$

$$v_x^{q+1}[m,n] = e^{-\alpha_x[m,n]\kappa\Delta t} v_x^q[m,n] - \frac{1 - e^{-\alpha_x[m,n]\kappa\Delta t}}{\delta\rho\kappa\alpha_x[m,n]}\left(p_x^q[m+1,n] - p_x^q[m,n] + p_y^q[m,n+1] - p_y^q[m,n]\right), \tag{A13}$$

$$v_y^{q+1}[m,n] = e^{-\alpha_y[m,n]\kappa\Delta t} v_y^q[m,n] - \frac{1 - e^{-\alpha_y[m,n]\kappa\Delta t}}{\delta\rho\kappa\alpha_y[m,n]}\left(p_x^q[m+1,n] - p_x^q[m,n] + p_y^q[m,n+1] - p_y^q[m,n]\right), \tag{A14}$$

which are the finite-difference formulations of acoustic PML.

APPENDIX B: RC FORMULATION FOR ACOUSTIC DRUDE AND LORENTZ DISPERSIVE MEDIUMS

By use of notation $p^q = p(q\Delta t)$, the finite-difference formulation of Eq. (20) can be written as

$$\kappa^{-1} * p^q = \kappa_\infty^{-1} p^q + \kappa_\infty^{-1}\sum_{s=0}^{q-1} p^{q-s}\int_{s\Delta t}^{(s+1)\Delta t}\chi(\tau)\mathrm{d}\tau. \tag{B1}$$

Similarly using $p^{q+1} = p(q\Delta t + \Delta t)$, we have

$$\kappa^{-1} * p^{q+1} = \kappa_\infty^{-1} p^{q+1} + \kappa_\infty^{-1}\sum_{s=0}^{q} p^{q-s+1}\int_{s\Delta t}^{(s+1)\Delta t}\chi(\tau)\mathrm{d}\tau, \tag{B2}$$

which can be rearranged as

$$\kappa^{-1} * p^{q+1} = \kappa_\infty^{-1} p^{q+1} + p^{q+1}\int_0^{\Delta t}\chi(\tau)\mathrm{d}\tau + \sum_{s=0}^{q-1} p^{q-s}\int_{(s+1)\Delta t}^{(s+2)\Delta t}\chi(\tau)\mathrm{d}\tau. \tag{B3}$$

Now subtract Eq. (B1) from Eq. (B3) to obtain

$$\kappa^{-1} * p^{q+1} - \kappa^{-1} * p^q = \kappa_\infty^{-1}(p^{q+1} - p^q) + \kappa_\infty^{-1} p^{q+1}\int_0^{\Delta t}\chi(\tau)\mathrm{d}\tau + \kappa_\infty^{-1}\sum_{s=0}^{q-1} p^{q-s}\left[\int_{(s+1)\Delta t}^{(s+2)\Delta t}\chi(\tau)\mathrm{d}\tau - \int_{s\Delta t}^{(s+1)\Delta t}\chi(\tau)\mathrm{d}\tau\right]. \tag{B4}$$

For convenience, define the parameter χ_s as

$$\chi_s = \int_{s\Delta t}^{(s+1)\Delta t} \chi(\tau)\mathrm{d}\tau, \tag{B5}$$

with which Eq. (B4) can be rewritten as

$$\begin{aligned} &\kappa^{-1} * p^{q+1} - \kappa^{-1} * p^q \\ &= \kappa_\infty^{-1}(1+\chi_0)p^{q+1} - \kappa_\infty^{-1}p^q + \kappa_\infty^{-1}\sum_{s=0}^{q-1} p^{q-s}(\chi_{s+1} - \chi_s). \end{aligned} \tag{B6}$$

Let $\Delta\chi_s = \chi_s - \chi_{s+1}$, and introduce the auxiliary variable S^q with the following definition:

$$S^q = \sum_{s=0}^{q-1} p^{q-s}\Delta\chi_s. \tag{B7}$$

The implicit formulation of p^{q+1} is then obtained from Eq. (B6) as

$$\begin{aligned} p^{q+1} &= \frac{1}{1+\chi_0}p^q + \frac{1}{1+\chi_0}S^q \\ &\quad + \frac{\kappa_\infty}{(1+\chi_0)}\left(\kappa^{-1} * p^{q+1} - \kappa^{-1} * p^q\right). \end{aligned} \tag{B8}$$

Substitute Eq. (B8) into dispersive acoustic Eq. (17) to achieve its finite-difference formulation

$$\begin{aligned} p^{q+1} &= \frac{1}{1+\chi_0}p^q + \frac{1}{1+\chi_0}S^q - \frac{\kappa_\infty}{1+\chi_0}\frac{\Delta t}{\delta} \\ &\quad \times \left(v_x^q[m+1,n] - v_x^q[m,n] + v_y^q[m,n+1] - v_y^q[m,n]\right). \end{aligned} \tag{B9}$$

The auxiliary variable S^q is to be determined by the specific dispersion model. Regarding the Drude dispersion having the form (8), the χ_s defined in Eq. (B5) is calculated to be

$$\begin{aligned} \chi_s &= \frac{\omega_c^2}{\gamma}\int_{s\Delta t}^{(s+1)\Delta t}(1 - e^{-\gamma\tau})d\tau \\ &= \frac{\omega_c^2}{\gamma}\Delta t - \frac{\omega_c^2}{\gamma^2}e^{-s\gamma\Delta t}(1 - e^{-\gamma\Delta t}), \quad s = 0, 1, \ldots. \end{aligned} \tag{B10}$$

The interval $\Delta\chi_s$ and its recursive formulation can be readily derived as

$$\Delta\chi_s = -\frac{\omega_c^2}{\gamma^2}e^{-s\gamma\Delta t}(1 - e^{-\gamma\Delta t})^2, \tag{B11}$$

$$\Delta\chi_{s+1} = \Delta\chi_s e^{-\gamma\Delta t}. \tag{B12}$$

By substitution of Eqs. (B10)–(B12) into Eq. (B7), the recursive formulation of the auxiliary variable S^q can be derived as

$$S^q = p^q\Delta\chi_0 + e^{-\gamma\Delta t}S^{q-1}, \tag{B13}$$

where the initial values of S^q are taken as $S^0 = S^1 = 0$.

Regarding the Lorentz dispersion, it is more convenient to compute S^q in the complex-value space.[38] Construct the complex function $\chi^C(t)$ according to $\chi(t) = Re[\chi^C(t)]$, so that expression (9) can be rewritten briefly as

$$\chi^C(t) = -j\alpha e^{(-\gamma + j\beta)t}. \tag{B14}$$

The complex functions corresponding to χ_s, $\Delta\chi_s$, and $\Delta\chi_{s+1}$ are easily calculated to be

$$\chi_s^C = \frac{-j\alpha}{\gamma - j\beta}e^{-s(\gamma - j\beta)\Delta t}\left[1 - e^{-(\gamma - j\beta)\Delta t}\right], \quad s = 0, 1, \ldots, \tag{B15}$$

$$\Delta\chi_s^C = \frac{-j\alpha}{\gamma - j\beta}e^{-s(\gamma - j\beta)\Delta t}\left[1 - e^{-(\gamma - j\beta)\Delta t}\right]^2, \tag{B16}$$

$$\Delta\chi_{s+1}^C = \Delta\chi_s^C e^{-(\gamma - j\beta)\Delta t}. \tag{B17}$$

By substitution of Eqs. (B15)–(B17) into Eq. (B7), the recursive formulation of S_C^q for the Lorentz dispersion is achieved

$$S_C^q = p^q\Delta\chi_0^C + e^{-(\gamma - j\beta)\Delta t}S_C^{q-1}, \tag{B18}$$

where the initial values of S_C^q take $S_C^0 = S_C^1 = 0$. Finally, S^q is received from $S^q = \mathrm{Re}[S_C^q]$.

[1] S. A. Cummer, J. Christensen, and A. Alù, "Controlling sound with acoustic metamaterials," Nature Rev. Mater. **1**, 16001 (2016).

[2] J. Christensen, M. Kadic, O. Kraft, and M. Wegener, "Vibrant times for mechanical metamaterials," MRS Commun. **5**(3), 453–462 (2015).

[3] G. Ma and P. Sheng, "Acoustic metamaterials: From local resonances to broad horizons," Sci. Adv. **2**(2), e1501595 (2016).

[4] Z. Liu, X. Zhang, Y. Mao, Y. Y. Zhu, Z. Yang, C. T. Chan, and P. Sheng, "Locally resonant sonic materials," Science **289**(5485), 1734–1736 (2000).

[5] Y. Lai, Y. Wu, P. Sheng, and Z. Q. Zhang, "Hybrid elastic solids," Nature Mater. **10**(8), 620–624 (2011).

[6] G. W. Milton and J. R. Willis, "On modifications of Newton's second law and linear continuum elastodynamics," Proc. R. Soc. London Ser. A **463**(2079), 855–880 (2007).

[7] S. Yao, X. Zhou, and G. Hu, "Experimental study on negative effective mass in a 1D mass–spring system," New J. Phys. **10**(4), 043020 (2008).

[8] H. H. Huang and C. T. Sun, "Wave attenuation mechanism in an acoustic metamaterial with negative effective mass density," New J. Phys. **11**(1), 013003 (2009).

[9] Z. Yang, J. Mei, M. Yang, N. Chan, and P. Sheng, "Membrane-type acoustic metamaterial with negative dynamic mass," Phys. Rev. Lett. **101**(20), 204301 (2008).

[10] C. J. Naify, C.-M. Chang, G. McKnight, and S. Nutt, "Transmission loss and dynamic response of membrane-type locally resonant acoustic metamaterials," J. Appl. Phys. **108**(11), 114905 (2010).

[11] N. Fang, D. Xi, J. Xu, M. Ambati, W. Srituravanich, C. Sun, and X. Zhang, "Ultrasonic metamaterials with negative modulus," Nature Mater **5**(6), 452–456 (2006).

[12] R. Gracia-Salgado, V. M. Garcia-Chocano, D. Torrent, and J. Sanchez-Dehesa, "Negative mass density and rho-near-zero quasi-two-dimensional metamaterials: Design and applications," Phys. Rev. B **88**(22), 224305 (2013).

[13] Z. Liang and J. Li, "Extreme acoustic metamaterial by coiling up space," Phys. Rev. Lett. **108**(11), 114301 (2012).

[14] Y. Xie, B.-I. Popa, L. Zigoneanu, and S. A. Cummer, "Measurement of a broadband negative index with space-coiling acoustic metamaterials," Phys. Rev. Lett. **110**(17), 175501 (2013).

[15] T. Frenzel, J. D. Brehm, T. Bueckmann, R. Schittny, M. Kadic, and M. Wegener, "Three-dimensional labyrinthine acoustic metamaterials," Appl. Phys. Lett. **103**(6), 061907 (2013).

[16]R. Zhu, X. N. Liu, G. K. Hu, C. T. Sun, and G. L. Huang, "Negative refraction of elastic waves at the deep-subwavelength scale in a single-phase metamaterial," Nat. Commun. **5**, 5510 (2014).
[17]J. Mei, G. Ma, M. Yang, Z. Yang, W. Wen, and P. Sheng, "Dark acoustic metamaterials as super absorbers for low-frequency sound," Nat. Commun. **3**, 756 (2012).
[18]A. N. Norris, "Acoustic cloaking theory," Proc. R. Soc. London Ser. A **464**(2097), 2411–2434 (2008).
[19]S. Zhang, C. Xia, and N. Fang, "Broadband acoustic cloak for ultrasound waves," Phys. Rev. Lett. **106**(2), 024301 (2011).
[20]B.-I. Popa, L. Zigoneanu, and S. A. Cummer, "Experimental acoustic ground cloak in air," Phys. Rev. Lett. **106**(25), 253901 (2011).
[21]J. Li, L. Fok, X. Yin, G. Bartal, and X. Zhang, "Experimental demonstration of an acoustic magnifying hyperlens," Nature Mater. **8**(12), 931–934 (2009).
[22]J. Zhu, J. Christensen, J. Jung, L. Martin-Moreno, X. Yin, L. Fok, X. Zhang, and F. J. Garcia-Vidal, "A holey-structured metamaterial for acoustic deep-subwavelength imaging," Nature Phys. **7**(1), 52–55 (2011).
[23]R. Fleury, D. L. Sounas, C. F. Sieck, M. R. Haberman, and A. Alù, "Sound isolation and giant linear nonreciprocity in a compact acoustic circulator," Science **343**(6170), 516–519 (2014).
[24]B.-I. Popa and S. A. Cummer, "Non-reciprocal and highly nonlinear active acoustic metamaterials," Nat. Commun. **5**, 3398 (2014).
[25]A. Archambault, M. Besbes, and J.-J. Greffet, "Superlens in the time domain," Phys. Rev. Lett. **109**(9), 097405 (2012).
[26]X. Zhou and G. Hu, "Analytic model of elastic metamaterials with local resonances," Phys. Rev. B **79**(19), 195109 (2009).
[27]S. Yao, X. Zhou, and G. Hu, "Investigation of the negative-mass behaviors occurring below a cut-off frequency," New J. Phys. **12**(10), 103025 (2010).
[28]S. H. Lee, C. M. Park, Y. M. Seo, Z. G. Wang, and C. K. Kim, "Acoustic metamaterial with negative modulus," J. Phys.: Condensed Matter **21**(17), 175704 (2009).
[29]A. Taflove and S. C. Hagness, *Computational Electrodynamics: The Finite-Difference Time-Domain Method*, 3rd ed. (Artech House, Norwood, MA, 2005), pp. 1–979.
[30]M. Orescanin, Y. Wang, and M. F. Insana, "3-D FDTD simulation of shear waves for evaluation of complex modulus imaging," IEEE Trans. Ultrason. Ferroelec. Freq. Control **58**(2), 389–398 (2011).
[31]X. L. Xi, Y. X. Du, J. F. Liu, and J. S. Zhang, "Unconditional stable FDTD method for modeling thin-film bulk acoustic wave resonators," IEICE Trans. Commun. **E95B**(12), 3895–3897 (2012).
[32]K. Kowalczyk and M. van Walstijn, "Room acoustics simulation using 3-D compact explicit FDTD schemes," IEEE Trans. Audio Speech Lang. Process. **19**(1), 34–46 (2011).
[33]X.-X. Su, J.-B. Li, and Y.-S. Wang, "A postprocessing method based on high-resolution spectral estimation for FDTD calculation of phononic band structures," Phys. B: Condensed Matter **405**(10), 2444–2449 (2010).
[34]Y. Xiaojuen, D. Borup, J. Wiskin, M. Berggren, and S. A. Johnson, "Simulation of acoustic wave propagation in dispersive media with relaxation losses by using FDTD method with PML absorbing boundary condition," IEEE Trans. Ultrason., Ferroelectr., Freq. Control **46**(1), 14–23 (1999).
[35]N. Jimenez, F. Camarena, J. Redondo, V. Sanchez-Morcillo, Y. Hou, and E. E. Konofagou, "Time-domain simulation of ultrasound propagation in a tissue-like medium based on the resolution of the nonlinear acoustic constitutive relations," Acta Acust. Acust. **102**(5), 876–892 (2016).
[36]Y. Kane, "Numerical solution of initial boundary value problems involving Maxwell's equations in isotropic media," IEEE Trans. Antennas Propag. **14**(3), 302–307 (1966).
[37]D. Botteldooren, "Finite-difference time-domain simulation of low-frequency room acoustic problems," J. Acoust. Soc. Am. **98**(6), 3302–3308 (1995).
[38]R. J. Luebbers and F. Hunsberger, "FDTD for Nth-order dispersive media," IEEE Trans. Antennas Propag. **40**(11), 1297–1301 (1992).
[39]R. Luebbers, D. Steich, and K. Kunz, "FDTD calculation of scattering from frequency-dependent materials," IEEE Trans. Antennas Propag. **41**(9), 1249–1257 (1993).
[40]D. R. Smith and D. Schurig, "Electromagnetic wave propagation in media with indefinite permittivity and permeability tensors," Phys. Rev. Lett. **90**(7), 077405 (2003).
[41]See supplementary material at http://dx.doi.org/10.1121/1.4971330 for animation plots of the pulse beam refraction in four different dispersion regimes.
[42]X. Zhou and G. Hu, "Superlensing effect of an anisotropic metamaterial slab with near-zero dynamic mass," Appl. Phys. Lett. **98**(26), 263510 (2011).
[43]P. Li, S. Yao, X. Zhou, G. Huang, and G. Hu, "Effective medium theory of thin-plate acoustic metamaterials," J. Acoust. Soc. Am. **135**(4), 1844–1852 (2014).
[44]J. P. Berenger, "A perfectly matched layer for the absorption of electromagnetic waves," J. Comput. Phys. **114**(2), 185–200 (1994).
[45]J. P. Berenger, "Perfectly matched layer for the FDTD solution of wave-structure interaction problems," IEEE Trans. Antennas Propag. **44**(1), 110–117 (1996).
[46]R. Holland, "Finite-difference time-domain (FDTD) analysis of magnetic diffusion," IEEE Trans. Electromag. Compatibil. **36**(1), 32–39 (1994).